

27.  $\beta$ -galactosidase activity was assayed as described by J. H. Miller [*Experiments in Molecular Genetics* (Cold Spring Harbor Laboratory, Cold Spring Harbor, NY, 1972)]. Cells to be assayed for  $\beta$ -galactosidase activity were cultured in the appropriate medium adjusted to pH 7.0, 0.1M potassium phosphate, and permeabilized with chloroform and sodium dodecyl sulfate.
28. C. R. Astell *et al.*, *Cell* **27**, 15 (1981).
29. M. N. Hall, C. Craik, G. Mullenbach, Y. Hiraoka, in preparation
30. T. Maniatis, E. F. Fritsch, J. Sambrook, *Molecular Cloning* (Cold Spring Harbor Laboratory, Cold Spring Harbor, NY, 1982).
31. G. F. Sprague and I. Herskowitz, *J. Mol. Biol.* **153**, 305 (1981).
32. D. W. Russell *et al.*, *Mol. Cell. Biol.* **6**, 4281 (1986).
33. E. Ciejek and J. Thorner, *Cell* **18**, 623 (1979); J. B. Hicks and I. Herskowitz, *Nature (London)* **260**, 246 (1976).
34. T. Manney and V. MacKay, personal communication.
35. We thank S. Michaelis and I. Herskowitz for strains; C. Keleher and E. Fodor for DNA fragments; P. O'Farrell, J. Theis, S. Fields, V. MacKay, L. Bell, T. Manney, R. Freedman, and J. Thorner for unpublished results; B. Sauer, P. Sternberg, S. Poole, P. O'Farrell, and S. Fried for comments on the manuscript, and H. Boyer for making this work possible. Supported by NIH grant GM35284 (M.N.H.) and by U.C. research grants (A.D.J.).

13 April 1987; accepted 6 July 1987

# Structure of the Nucleotide Activation Switch in Glycogen Phosphorylase a

STEPHEN SPRANG, ELIZABETH GOLDSMITH, ROBERT FLETTERICK

Adenosine monophosphate is required for the activation of glycogen phosphorylase b and for release of the inhibition of phosphorylase a by glucose. Two molecules of adenosine monophosphate (AMP) bind to symmetry related sites at the subunit interface of the phosphorylase dimer. Adenosine triphosphate (ATP) binds to the same site, but does not promote catalytic activity. The structure of glucose-inhibited phosphorylase a bound to AMP and also of the complex formed with glucose and ATP is described. Crystallographic refinement of these complexes reveals that structural changes are associated with AMP but not ATP binding. The origin of these effects can be traced to different effector binding modes exhibited by AMP and ATP, respectively. The conformational changes associated with AMP binding traverse multiple paths in the enzyme and link the effector and catalytic sites.

GLYCOGEN PHOSPHORYLASE (GP) MOBILIZES GLUCOSE-1-phosphate (G1P) in eukaryotes and is regulated by two parallel mechanisms. The primary control, common to all of the tissue specific isozymes, occurs through phosphorylation of the GP dimer by a specific kinase (1), which is in turn regulated via extracellular neural and hormonal signals. A second, intracellular control is exerted through the cooperative binding of adenosine monophosphate (AMP) to the unphosphorylated enzyme phosphorylase b (GPb). The mechanism and efficiency of AMP activation varies among the tissue isozymes (2). Binding of AMP to one subunit of muscle GPb both promotes the binding of AMP to the second subunit (3) and activates the dimer for substrate binding and

catalysis. GPb is inactive in the absence of AMP (4) and is 80 percent as active as the phosphorylated enzyme, phosphorylase a (GPa) (5) in its presence.

Phosphorylase a functions efficiently in the absence of AMP, although AMP activates at low substrate concentrations (6) and releases the enzyme from glucose inhibition (7). AMP binds to GPa

Table 1. Crystallographic data and refinement results.

Crystal data							
Lig- and	No. of crys- tals	Reflections*		$R_m^\dagger$	Cell (Å)‡		rms§ $\Delta F/F$ (%)
		Total	Accepted		a	c	
AMP	14	16,203	12,442	0.030	128.3	117.0	14.0
ATP	14	16,398	12,615	0.022	128.2	117.0	6.0

Refinement results			
Ligand	$R_{\text{cryst}}  $	$\Delta$ bond¶ (Å)	$\Delta$ angle (Å)
AMP	0.12	0.02	0.04
ATP	0.11	0.02	0.04

\*Reflections were accepted for inclusion in the data set if  $I_{hkl}/\sigma_I > 3.0$ , where  $I_{hkl}$  is the measured intensity and  $\sigma_I$  is the standard error. †A set of common scaling reflections is measured for each crystal (data set); the agreement among sets is given by the merging index:

$$R_{\text{merge}} = \frac{\sum_{hkl} \sum_n (I_{hkl}^n - I_{hkl}) / I_{hkl}}{\sum_{hkl} I_{hkl}}$$

where  $I_{hkl}^n$  are the intensities of scaling reflections for the  $n$ th crystal and  $I_{hkl}$  is the mean intensity. The summation is taken over the  $N$  measurements of (hkl). ‡Cell constants for the parent GP crystals containing glucose at the catalytic site are  $a = b = 128.4$  Å and  $c = 116.4$  Å. §The root mean square (rms) difference in observed scattering amplitude with respect to parent crystals. ¶The crystallographic  $R$  factor is a measure of agreement between observed ( $|F(\text{obs})_{hkl}|$ ) structure factor amplitudes and amplitudes ( $|F(\text{calc})_{hkl}|$ ) calculated from the atomic model:

$$R_{\text{cryst}} = \frac{\sum_{hkl} (||F(\text{obs})_{hkl}| - |F(\text{calc})_{hkl}||)}{\sum_{hkl} |F(\text{obs})_{hkl}|}$$

¶The mean deviation between bond distances ( $\Delta$  bond) in the refined model and ideal bond distances, and the corresponding mean deviation between bond angle distances ( $\Delta$  angle) and ideal angle distances.

The authors are at the Department of Biochemistry, University of California, San Francisco, CA 94143. The present address of S. Sprang and E. Goldsmith is Department of Biochemistry, The University of Texas Health Science Center at Dallas, Howard Hughes Medical Institute, 5323 Harry Hines Boulevard, Dallas, TX 75235-9050.

three orders of magnitude more tightly than to GPb (5), although unlike GPb, without cooperativity between subunits.

The nucleotide site in GP binds and discriminates between the activators AMP and inosine monophosphate (IMP) and inhibitors adenosine triphosphate (ATP) and glucose-6-phosphate (G6P) (2). Both ATP and G6P inhibit GPb by competing with AMP and they stabilize the catalytically inactive (T state) conformation. Through its response to intracellular ratios of these effector molecules, the activity of GP is tailored to the metabolic state of the cell.

Earlier crystallographic studies resulted in the characterization of the nucleotide binding site in GPa (8) and GPb (9). The interaction of AMP, ATP, and G6P with GPb has been discussed in detail (10, 11). However, the structural basis for parallel regulation by phosphorylation and AMP, the ability of the enzyme to discriminate

between activators and inhibitors at the nucleotide site, and the mechanism by which conformational signals originating from the nucleotide site are communicated to the catalytic site some 40 Å away, are all poorly understood. To address these problems, we present the refined structures of GPa complexed with AMP and of GPa bound to ATP, both in the presence of the inhibitor glucose bound at the active site. Under these conditions AMP binds cooperatively and activates GP while ATP binds but does not activate the enzyme.

**Structural determination.** Parent crystals of GPa containing glucose bound at the active site (12) were soaked in buffer (13) containing AMP or ATP to form nucleotide complexes. Of the total observable x-ray data, the most intense 40 to 60 percent was measured by diffractometer to a maximum resolution of 2.5 Å (12, 14). Merging statistics for reflections measured in common for each

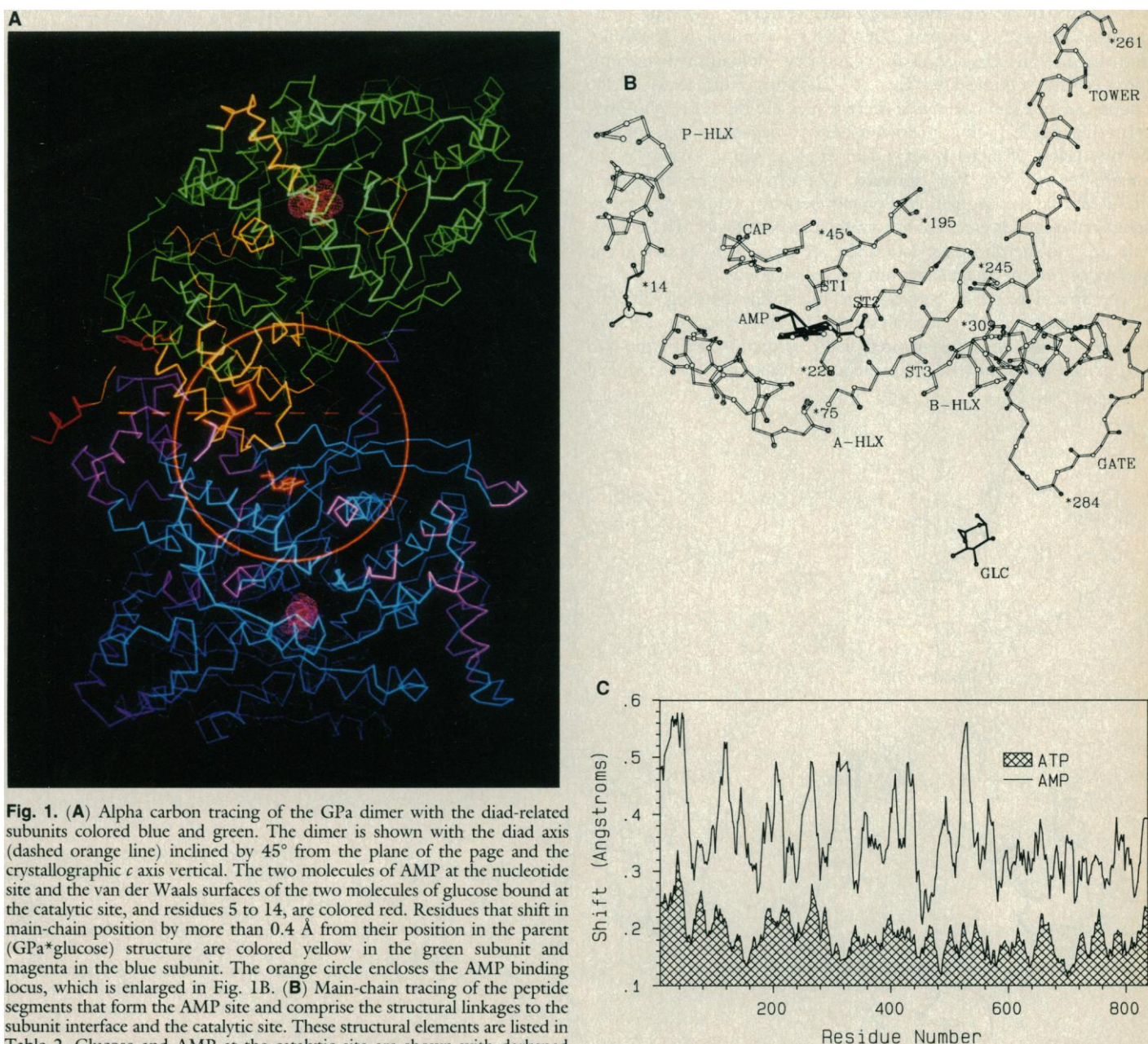


**Fig. 1.** (A) Alpha carbon tracing of the GPa dimer with the diad-related subunits colored blue and green. The dimer is shown with the diad axis (dashed orange line) inclined by 45° from the plane of the page and the crystallographic *c* axis vertical. The two molecules of AMP at the nucleotide site and the van der Waals surfaces of the two molecules of glucose bound at the catalytic site, and residues 5 to 14, are colored red. Residues that shift in main-chain position by more than 0.4 Å from their position in the parent (GPa\*glucose) structure are colored yellow in the green subunit and magenta in the blue subunit. The orange circle encloses the AMP binding locus, which is enlarged in Fig. 1B. (B) Main-chain tracing of the peptide segments that form the AMP site and comprise the structural linkages to the subunit interface and the catalytic site. These structural elements are listed in Table 2. Glucose and AMP at the catalytic site are shown with darkened bonds. Carbon atoms are shown as small empty circles, nitrogen atoms as larger circles, and oxygen atoms as larger, filled circles. (C) A plot of the shift in main-chain position from the parent structure as a function of sequence number. The value plotted for each residue is a local average over the 15

residues nearest in primary sequence. The root-mean-square difference in atomic position of main-chain atoms is 0.35 Å for parent versus the GPa\*AMP\*glucose complex and 0.17 Å for parent versus the GPa\*ATP\*glucose complex.

crystal are given in Table 1. Preliminary positions of the bound ligands were determined from difference Fourier maps, calculated with coefficients ( $F_{\text{ligand}} - F_{\text{parent}}$ ), and crystallographic phases were computed from the atomic model of the parent structure (excluding bound water molecules). The parent structure has been refined against x-ray data extending to 2.1 Å resolution to a crystallographic  $R$  factor of 0.15 (15). Atomic coordinates for the ligands used to fit the difference electron density were taken from single crystal x-ray diffraction studies (16).

Atomic coordinates and temperature factors for the complexes of GP<sub>a</sub> with AMP or ATP were subjected to cycles of stereochemically restrained crystallographic refinement (17, 18) alternating with manual refitting of the model to the electron density with the use of the molecular model building program FRODO (19) (Table 1).

**Structural context of the nucleotide binding site.** Phosphorylase a crystallizes with the twofold axis of the dimer coincident with a symmetry element of the  $P4_32_12$  unit cell (Fig. 1A). The phosphorylase subunit is comprised of a COOH-terminal, or "catalytic" domain, and an NH<sub>2</sub>-terminal, "regulatory" domain, which forms most of the subunit interface (20, 21) and is the locus of the oligosaccharide and nucleotide effector sites and the site of phosphorylation at Ser<sup>14</sup>. Each domain consists of a beta-sheet core covered by two layers of alpha helices. The catalytic site is located in the crevice between the two domains. Contacts between monomers occur across the regulatory domain between regular secondary structural elements emanating from the beta-sheet core. The nucleotide site and the phosphorylation site are proximally located at the surface of the enzyme and within the subunit interface.

The spatial relations between the nucleotide binding site, the subunit interface, and the catalytic site are shown in Fig. 1B. The nucleotide binding site is situated at the vertex formed by the two helices labeled A and B. These helices traverse the NH<sub>2</sub>-terminal

domains of each subunit of the phosphorylase dimer and form part of the floor of the nucleotide binding site. Residues 42' to 45' (residues of the twofold related subunit are designated by prime numbers) which precede the A helix of the twofold related subunit cap the binding site. Thus, the bound effector bridges and mediates contacts between subunits. The relation between the nucleotide site and the locus of the phosphorylation is shown in Fig. 2A; AMP binds only 10 Å from the phosphoserine in GP<sub>a</sub>, which plays a similar structural role by linking the cap of one subunit with the A helix of the molecule related by the twofold axis (21).

The nucleotide binding site forms part of the subunit interface and is in protein-mediated contact with the catalytic site (Fig. 1B and Table 2). Three β strands (ST1 to 3) in the regulatory domain beta sheet underlie the AMP site. The beta sheet is linked to the AMP site and subunit interface through a buried salt bridge between Lys<sup>41'</sup> and Glu<sup>195</sup>. Helix B connects the nucleotide binding site with the catalytic site through the hairpin gate (residues 282 to 285) that blocks the catalytic site from the solvent exterior. The two active site gates of the dimer are linked through packing interactions between the diad related tower helices (residues 261 to 277), and the tower helix itself makes intimate contact with ST3.

**Binding interactions of AMP and ATP.** The A and B helices are linked to the cap by AMP through specific hydrogen bond and van der Waals interactions. The nucleotide binding locus consists of three subsites (Table 3) that interact with the purine, ribosyl, and monophosphate or triphosphate groups of the ligand. The purine binding site consists of Tyr<sup>75</sup> and Asn<sup>44'</sup>. When AMP is bound, Tyr<sup>75</sup> is rotated from its position in the parent structure (Fig. 2A), and is partially stacked over the adenine ring (Fig. 2B). The tyrosyl and adenine rings are nearly parallel and approach within 3.4 Å; Tyr<sup>75</sup> is partially disordered in the parent crystals, but is localized as a result of AMP binding. A distorted and presumably weak hydro-

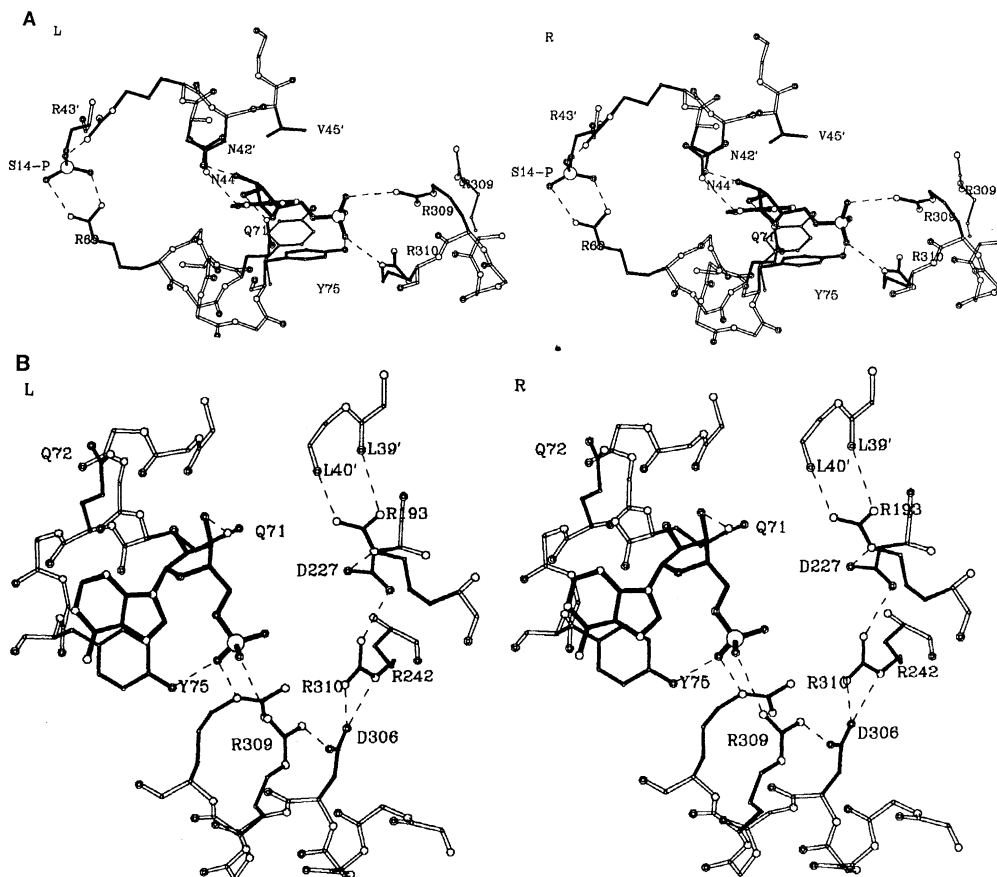


**Fig. 2.** (A) Stereoscopic view along the crystallographic  $b$  axis of the AMP binding site showing its relationship to the phosphoserine-14 binding site. Thin bonds show the positions of Tyr<sup>75</sup> and Arg<sup>310</sup> in the parent structure. Hydrogen bonds are represented as dashed lines and atom type is coded as in Fig. 1B. (B) View perpendicular to (A), along the crystallographic  $c$  axis. Residues of the cap have been omitted. The chain of salt bridges and hydrogen bonds is shown linking residues 39' and 40' to Arg<sup>193</sup>, Asp<sup>227</sup>, and Arg<sup>242</sup> from ST1, ST2, and ST3, respectively, and to the AMP site residues Asp<sup>306</sup> and Arg<sup>309</sup>.

gen bond between the O $\delta$ 1 atom of Asn<sup>44'</sup>, and the purine N3 atom constitutes the only other interaction involving the purine ring.

The AMP ribosyl group is bound in a groove of the A helix flanked by residues 71 and 72 (Fig. 2B) and contacts the cap (residues 42' to 45') of the opposite subunit. The Gln<sup>72</sup> is hydrogen bonded to the ribosyl 3' hydroxyl group, while the ribosyl 2' hydroxyl group donates a hydrogen bond to Asp<sup>42'</sup>. The ribosyl 2' methylene group is within van der Waals contact distance of Val<sup>45'</sup>.

The AMP phosphate group forms two ion pairs, one with Arg<sup>309</sup> and a second with Arg<sup>310</sup>. The Arg<sup>310</sup> side chain rotates nearly 45° about the C $\alpha$ -C $\beta$  bond from its position in the parent structure on binding AMP. The hydroxyl group of Tyr<sup>75</sup> is hydrogen bonded to a phosphate oxygen atom of AMP, thus Tyr<sup>75</sup> interacts at both the base and phosphate subsite. The ion pair interactions involving the AMP phosphate group augment a chain of electrostatic interactions linking the edge of the beta sheet to the AMP site (Fig. 2A).

ATP occupies the same site as does AMP, but interacts differently with binding site residues (Fig. 3). Only the triphosphate group of ATP makes significant contact with the enzyme (Table 3). The phosphodiester linkage between the  $\alpha$ - and  $\beta$ -phosphate atoms of ATP occupies the same position as the  $\alpha$ -phosphate group of AMP (Fig. 4). Both Arg<sup>309</sup> and Arg<sup>310</sup> form contacts with  $\alpha$ - and  $\beta$ -phosphate oxygen atoms (Table 2). The additional two units of formal charge carried by ATP relative to AMP may be compensated

by ion pairs with Lys<sup>41'</sup> and Arg<sup>242</sup>, which do not occur in the AMP complex. In the AMP complex, Arg<sup>309</sup> interacts with both the nucleotide phosphate and Asp<sup>306</sup>, whereas in the ATP complex it forms only a single bi-dentate salt bridge with the  $\beta$ -phosphate of ATP and does not compensate the charge on Asp<sup>306</sup>.

In binding ATP, the nucleotide site accommodates a triphosphate group at the same locus to which the AMP monophosphate is bound. Consequently, the nucleotide moiety of ATP is thrust toward the solvent exterior relative to the position occupied by that group in the AMP complex. The ATP adenine ring is not in van der Waals or hydrogen bond contact with the enzyme and is disordered. The ribosyl group of ATP is well ordered but forms only one interaction with the protein, a hydrogen bond between O3' and Gln<sup>72</sup> O $\delta$ 1.

The molecular conformations of AMP and ATP are similar to those reported for the GPb complexes (10, 11). The two ligands differ only in that the ribosyl group of AMP is puckered C2'-endo, whereas ATP is puckered C3'-endo. The glycosyl conformation (anti) and the torsion angles about the phosphodiester linkages for both AMP and ATP are well within the ranges observed in crystal structures of nucleotides and their analogs (22); there is no evidence that the ligands are conformationally strained within the enzyme binding site.

**Protein conformational changes.** The binding of AMP to GP $\alpha$

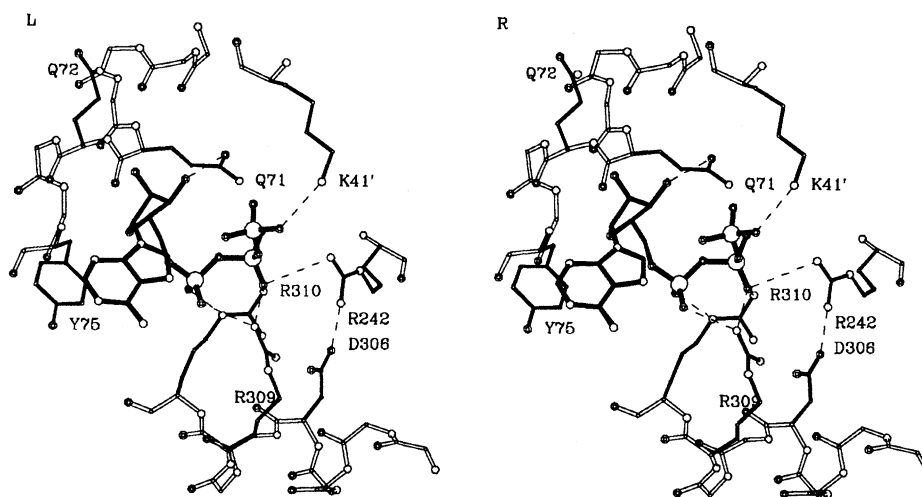


**Fig. 3.** Stereoscopic view down the crystallographic  $a$  axis of ATP bound to the nucleotide site. There is a salt bridge between Lys<sup>41'</sup> of the twofold related molecule and the phosphate group of ATP. In this complex, there is no salt bridge from Asp<sup>306</sup> to Arg<sup>309</sup> as in the ATP complex.

**Table 2.** Structural elements involved in AMP binding and activation.

Element name	Residues	2°* Str	AMP† binding	Structural linkages
P helix	1-14	$\alpha$		Ser-14-P
Cap	42-45	t	+	Subunit interface
A helix	48-80	$\alpha$	+	Ser-14-P
Mg <sup>2+</sup> site	95-126	$\alpha\tau\alpha\alpha$		Subunit interface
B helix	287-313	$\alpha$	+	Gate-tower
Strand 1 (ST1)	189-193	$\beta$		Subunit interface
Ribbon	195-219	( $\beta_2$ )		Glycogen binding
Strand 2 (ST2)	220-229	$\beta$		Subdomain-subunit interface
Strand 3 (ST3)	235-247	$\beta$	(ATP)	ST1-subunit interface
Tower	261-277	$\alpha$		Gate-subunit interface
Gate	282-285	( $\epsilon_2$ )		Active site
Glycogen				
Binding sub-domain	387-438	$\beta\alpha_3\beta_2$		Active site-subunit interface

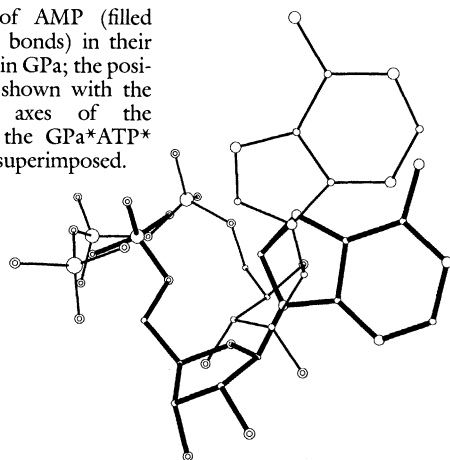
\* $\alpha$ , Alpha helix;  $\beta$ , beta strand;  $\epsilon$ , extended; t, turn; antiparallel hairpin structures are enclosed in parentheses. †Elements marked (+) contain AMP-binding residues.

**Table 3.** Intermolecular contacts between AMP, ATP, and phosphorylase a.

Protein atom	AMP/ATP atom	AMP distance (Å)	ATP distance (Å)
		<i>Ribose</i>	
Asp <sup>42'</sup> O $\delta$ 1	O2'	2.6	3.4
Val <sup>45'</sup> C $\gamma$ 1	C2'	3.1	
Gln <sup>71</sup> N $\epsilon$ 2	O3'	2.6	3.3
		<i>Purine</i>	
Asn <sup>44'</sup> O $\delta$ 1	N3	3.0	
Tyr <sup>75*</sup>		3.4	
		<i>Phosphates</i>	
Tyr <sup>75</sup> O $\eta$	O11	2.6	
Arg <sup>242</sup> N $\eta$ 2	O22		3.7
Arg <sup>309</sup> N $\eta$ 1	O111	3.2	
Arg <sup>309</sup> N $\eta$ 2	O22		2.4
	O1		2.8
Arg <sup>310</sup> N $\epsilon$	O11	3.0	2.7
Arg <sup>310</sup> N $\eta$ 2	O22		3.9
Lys <sup>41'</sup> N $\zeta$	O33		3.5

\*Value shown is the mean of the distances between each purine atom and the closest form of Y75. Distances greater than 4.0 Å are not considered. Because the purine ring of ATP is disordered, distances are not computed.

**Fig. 4.** Superposition of AMP (filled bonds) and ATP (empty bonds) in their respective binding modes in GPa; the positions of the ligands are shown with the origins and unit-cell axes of the GPa\*AMP\*glucose and the GPa\*ATP\*glucose complex crystals superimposed.



in the presence of glucose results in small but long-range conformational changes that affect interactions between the subunits and between the protein domains that surround the catalytic site. Although the displacement magnitudes for many residues are within the range of precision with which atomic coordinates can be accurately determined at 2.5 Å resolution, the strong correlations in the shifts of neighboring residues (spatially and in primary sequence) indicate that the displacements are due to ligand binding rather than experimental error or refinement artifacts. Whereas both AMP and ATP binding results in local rearrangements within the binding site, global conformational changes are observed only with AMP (Fig. 1C).

The reorientations of Tyr<sup>75</sup> and Arg<sup>309</sup> described above are the most dramatic of those observed within the binding site. In the AMP complex, Gln<sup>71</sup> and the cap also shift to form hydrogen bonds and van der Waals contacts with the ligand. Global conformational changes in the GPa\*AMP\*glucose complex consist of small (0.2 Å to 0.75 Å) correlated shifts of secondary structural elements both immediately surrounding and distant from the binding site.

Conformational changes that emanate from the binding site affect the entire subunit interface and, to a lesser extent, the catalytic site. The cap approaches the A helix of the twofold related subunit as AMP is bound between them. Consequently, the subunits move toward each other, as is evident in the shift vector diagrams in Fig. 5, A and B. The A helix bends slightly as its NH<sub>2</sub>- and COOH-termini are displaced toward the AMP sites, and the turn of helix encompassed by residues 60 to 65 winds up slightly through small changes in the  $\phi$  and  $\psi$  angles at residue 63. The NH<sub>2</sub>-terminal helix (residues 5 to 13) and the phosphoserine shift slightly toward the protein surface. The distance between the oxygen atoms of the phosphoserine phosphate and the hydrogen bond donor groups of Arg<sup>69</sup> and Arg<sup>43</sup> decrease by an average of 0.2 Å when AMP, but not ATP, is bound—a possible indication that only AMP strengthens the interactions between the phosphoserine residue and its binding site at the subunit interface.

Two helices (Table 2) that comprise the magnesium ion binding site participate in the transmission of conformational changes to the catalytic site (8, 21) and make numerous contacts with the first 70 residues of the enzyme. The second helix in the Mg<sup>2+</sup> binding site is connected to an alpha helix (residues 134 to 152) that binds substrate phosphate at the catalytic site. The loop (residues 115 to 117) connecting the Mg<sup>2+</sup> binding helices makes hydrophobic contacts with the NH<sub>2</sub>-terminus of the A helix and with the NH<sub>2</sub>-terminal helix (5 to 13) of the opposite subunit. These contacts are preserved as the A helix moves toward the subunit interface, carrying the Mg<sup>2+</sup> binding site with it. The shift vector diagram

(Fig. 5A) shows that the active site helix rides on the motion of the Mg<sup>2+</sup> binding helices at the subunit interface. Magnesium ions have been shown to promote AMP binding cooperatively in the absence of substrates (23).

The first three strands of the regulatory domain beta sheet are also involved in communication between subunits. Hydrogen bonds link Arg<sup>193</sup> in the helical turn following ST1 (Table 2 and Fig. 2B) to the main-chain carbonyl oxygen atoms of residues 39' to 40', which precede the AMP binding cap in the twofold related subunit. Lysine-41' also forms a salt bridge with Glu<sup>195</sup>. A second link is forged through direct van der Waals contact (via Tyr<sup>194</sup> and Pro<sup>185</sup>) between ST1 and its counterpart in the opposite subunit. The interstrand interactions are tightened, and the ST1 cap bridge is preserved as the subunits move together on AMP binding (Fig. 5B).

Closure of the subunit interface also occurs along the opposite side of the molecule from the AMP site (Fig. 5B). The tower helix packs at a 160° angle against its counterpart in the twofold related subunit through a series of interdigitating side chains. When AMP is bound, the helices move along one another, each toward the opposite subunit. Communication between the AMP site and the tower is mediated by structural changes involving ST1 to ST3. These strands form the floor of the AMP site and are linked together by main-chain hydrogen bonds and by electrostatic interactions between the side chains of residues Glu<sup>193</sup>, Asp<sup>227</sup>, and Arg<sup>242</sup> which contact residues in the AMP binding site (Fig. 2B). Side chains of the tower helix are hydrogen bonded to main-chain atoms of the ST3. The tower helix leads to the active site gate which, when substrates are bound, is displaced or disordered (24). Movement of the tower helix toward the subunit interface and away from the catalytic site may be a direct mechanism by which AMP opens the active site and promotes substrate binding. Because glucose is bound within the active site and is hydrogen-bonded to Asn<sup>284</sup> (25), the gate is not disordered in the GPa\*AMP\*glucose complex.

Long-range conformational changes are described by changes in distances between centroids of secondary structural elements (alpha helices and beta strands) within and between subunits. Secondary structural elements that pack so that they are adjacent to one another within the monomer do not undergo significant changes in separation. In contrast, distances between elements in different domains or different structural units within the same domain change by as much as 0.3 Å. This indicates that global conformational changes are achieved through the vectorial addition of small rearrangements at residue packing interfaces (26). Most of the structural changes can be accounted for by grouping the subunit into 14 covalently connected peptides that move approximately as units (Fig. 6A).

Matrix analysis of inter-unit distances demonstrates that the structural units that form the subunit interface of one monomer move together (units I1 to I2 and I4 to G1, Fig. 6A) as the interactions between subunits are tightened. The glycogen binding domain (units G1 to G4) rotates away from the subunit interface (units I4 to I5) and from the surface of the catalytic domain (units C1 to C4). The interface segment, unit I5, which contains the tower helix moves away from the catalytic domain. The COOH-terminus, unit T, becomes more tightly associated with the glycogen binding subdomain (units G1 to G4) and the catalytic domain (units C1 to C4). These shifts contribute to a global increase in separation between the NH<sub>2</sub>- and COOH-terminal domains within monomers and between the COOH-terminal domains in opposite subunits concurrent with the movement of the interface structures toward each other. While no dramatic structural changes are evident within the catalytic site itself, the overall effect of these small global changes is to increase the accessibility of the active site.

**Mechanism of nucleotide activation.** In analogy to the active

site of GP, which is complementary to the inhibitor glucose in the T state (26) and to G1P in the catalytically active R state (24), the effector site of the nucleotide is able to recognize activators (that is, AMP and IMP) and inhibitors (ATP and G6P). The structural basis of dual recognition lies in the plasticity of the binding site. The activator AMP is able to bind to either active or inactive phosphorylase conformers, although it derives the maximum binding energy through interaction with the activated state.

AMP activates GP by promoting tighter interactions between subunits while relaxing interactions between domains, thereby allowing the catalytic site to open. Although of small magnitude, conformational changes induced in glucose-inhibited GP<sub>a</sub> traverse multiple paths through which the AMP sites in each subunit communicate with one another and with the catalytic sites. Preservation of the twofold symmetry at the subunit interface rationalizes cooperativity between AMP sites, since the cap-A-helix unit that forms the roof of one AMP site is also the floor of the diad-related site. On binding AMP, residues at the binding site undergo conformational rearrangements. Through preservation of existing

packing interactions with residues surrounding the binding pocket, conformational changes are communicated to structural elements distant from the binding site. Changes are manifested as gradual deformations of loosely packed segments of beta sheet and alpha helix that are rigid enough to move as units but are not firmly tethered within the tertiary structure.

Activation by phosphorylation at Ser<sup>14</sup> parallels that induced by AMP binding. The two events promote similar rearrangements within the same structural elements (27). In GP<sub>a</sub>, phosphoserine-14 forms ion pairs with Arg<sup>43</sup> and Arg<sup>69</sup> (21), thus pulling the cap at the NH<sub>2</sub>-terminus of the A helix of one subunit toward the COOH-terminus of the corresponding helix in the opposite subunit. The AMP promotes the same structural changes by interacting with different residues in the cap site and the A helix. GP<sub>b</sub> binds AMP cooperatively because binding energy is used to stabilize an active conformation that is also more complementary to AMP. Phosphorylation of the enzyme also stabilizes the high affinity form, thus all of the energy gained through ligand interaction is expressed as binding affinity.

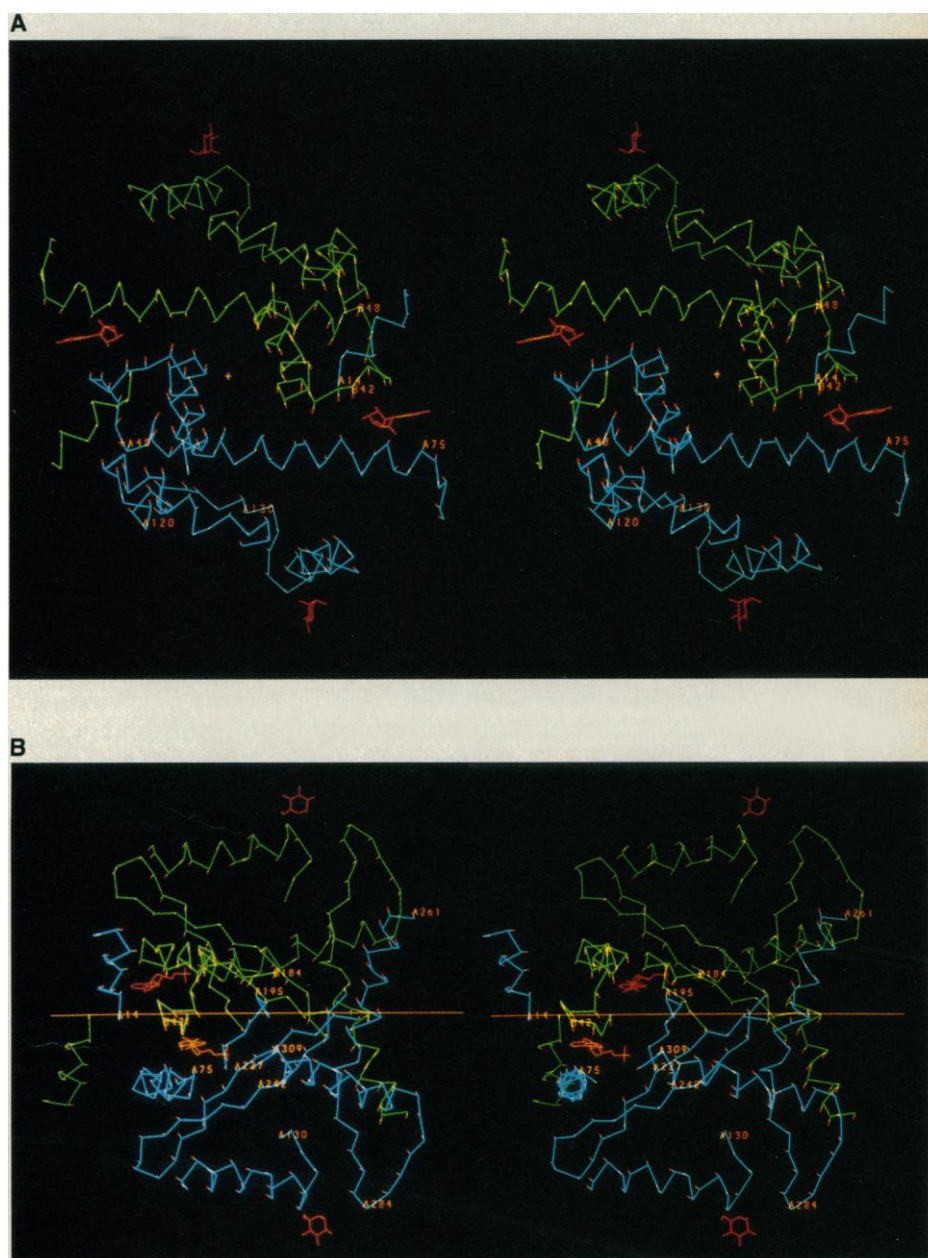


**Fig. 5.** Structural rearrangements of GP<sub>a</sub> induced by AMP (red) in the presence of glucose (red) at the active site. Color coding is the same as in Fig. 1B. The shift of each residue is shown as a red vector with its origin at C $\alpha$  pointing in the direction of the shift. The vector length is scaled to three times the magnitude of the displacement. (A) Stereoscopic view along the twofold axis (marked with a "+") of the GP dimer, which bisects the crystallographic *a* and *b* axes. (B) View with the twofold axis, shown as an orange line, horizontal. For clarity, the NH<sub>2</sub>-terminus of the A-helix cap in the blue subunit and the COOH-terminus of the A helix in the green subunit have been omitted.



- (1967); P. J. Kasvinsky, N. B. Madsen, J. Sygusch, R. J. Fletterick, *ibid.* **253**, 3343 (1978).
9. I. T. Weber *et al.*, *Nature (London)* **274**, 433 (1978).
  10. L. N. Johnson *et al.*, *J. Mol. Biol.* **134**, 639 (1979).
  11. E. A. Stura *et al.*, *ibid.* **170**, 529 (1983).
  12. R. J. Fletterick *et al.*, *ibid.* **103**, 1 (1976).
  13. Soaking buffer contained 10 mM 2-[bis(2-hydroxyethyl)amino]ethanesulfonic acid, pH 6.8, 10 mM magnesium acetate, 0.1 mM EDTA, 0.1 mM dithiothreitol (DTT), and 50 mM  $\alpha$ -D-glucose and either 0.5 mM AMP or 20 mM ATP. Parent crystals were soaked for 12 to 24 hours at 22°C.
  14. R. J. Fletterick and J. Sygusch, *Methods Enzymol.* **114**, 386 (1985).
  15. S. R. Sprang, E. J. Goldsmith, R. J. Fletterick, unpublished data.
  16. Coordinates of AMP in the C(3)-endo conformation taken from J. Kraut and L. Jensen [*Acta Crystallogr.* **16**, 79 (1963)]; for the C(2)-endo conformer from S. Neidle [*ibid.* **32**, 1580 (1976)]. Coordinates for ATP are from the determination by D. Kennard *et al.* [*Proc. R. Soc. London Ser. A* **325**, 401 (1971)].
  17. W. A. Hendrickson and J. H. Konnert, in *Biomolecular Structure, Function, Conformation, and Evolution*, R. Srinivasan, Ed. (Pergamon, New York, 1981), vol. 1, p. 43.
  18. We used a version of the Hendrickson-Konnert program modified by D. Rees and M. Lewis to compute the gradient-curvature matrix directly from difference Fourier maps. Weights ( $W$ ) for individual reflections were set to unity. Crystallographic terms were weighted by setting the Hendrickson-Konnert program parameter AFSIG to a value of 20, where  $AFSIG(=1/W^2)$  relative to unit weights for all stereochemical terms. Thermal factor refinement was introduced after cycle 30 in the refinement of coordinates for the AMP complex and after cycle 9 for the ATP complex. The refinement method restrains variations in B factors among atoms separated by one to three bonds. Final atomic coordinates for AMP and ATP were obtained by omitting the preliminary ligand coordinates from the phasing model during the last three cycles of refinement. The model of AMP or ATP was then fit into the residual electron density of the  $|F_{obs}| - |F_{calc}|$  map computed with refined phases. The fit of the model to the density was refined manually by rotations about extracyclic single bonds.
  19. T. A. Jones, *Acta Crystallogr.* **11**, 268 (1978); J. W. Pflugrath, M. A. Saper, F. A. Quiocho, in *Methods and Applications in Crystallographic Computing*, S. Hall and T. Ashidajeds, Eds. (Oxford Univ. Press, New York, 1984), p. 404.
  20. S. R. Sprang and R. J. Fletterick, *J. Mol. Biol.* **131**, 523 (1979).
  21. ———, *Biophys. J.* **32**, 175 (1980).
  22. M. Sundaralingam, *Jerusalem Symp. Quant. Chem. Biochem.* **5**, 417 (1973).
  23. L. L. Kastenschmidt, J. Kastenschmidt, E. Helmreich, *Biochemistry* **1**, 4543 (1968).
  24. S. G. Withers, N. B. Madsen, S. R. Sprang, R. J. Fletterick, *ibid.* **21**, 5372 (1982).
  25. S. R. Sprang, E. J. Goldsmith, R. J. Fletterick, S. G. Withers, N. B. Madsen, *ibid.*, p. 5364.
  26. A. Lesk and C. Chothia, *J. Mol. Biol.* **174**, 175 (1984).
  27. S. R. Sprang, E. Goldsmith, R. Fletterick, R. Achari, L. Johnson, unpublished results.
  28. A. Lorek *et al.*, *Biochem. J.* **218**, 45 (1984).
  29. R. J. Fletterick and S. R. Sprang, unpublished results.
  30. J. H. Wang and W. J. Black, *J. Biol. Chem.* **17**, 4641 (1968).
  31. B. Vandenburg, M. Dreyfus, H. Buc, *Biochemistry* **17**, 4153 (1978).
  32. N. B. Madsen, P. J. Kasvinsky, R. J. Fletterick, *J. Biol. Chem.* **253**, 9097 (1978).
  33. Supported by NIH grants GM00085-05 (R.J.F.) and DK31507-05 (S.R.S.). We thank N. Madsen for helpful discussions and for providing the parent crystals used in the analysis, and Naomi Ervin for assistance with preparation of the manuscript. Coordinates of the refined protein complexes will be deposited at the Brookhaven Protein Data Bank.

23 March 1987; accepted 22 July 1987

